

## Structural and electrical properties of intercalated and ion-implanted highly ordered graphite fibers

M. Endo

*Faculty of Engineering, Shinshu University, Nagano 380, Japan\* and Center for Materials Science and Engineering, Massachusetts Institute of Technology, Cambridge, Massachusetts 02139*

T. C. Chieu,<sup>†</sup> G. Timp,<sup>†</sup> and M. S. Dresselhaus

*Department of Electrical Engineering and Computer Science and Center for Materials Science and Engineering, Massachusetts Institute of Technology, Cambridge, Massachusetts 02139*

B. S. Elman

*Department of Physics and Center for Materials Science and Engineering, Massachusetts Institute of Technology, Cambridge, Massachusetts 02139*

(Received 22 November 1982; revised manuscript received 25 July 1983)

Because of their high degree of structural order, high mechanical strength, and small diameter ( $\sim 1 \mu\text{m}$ ), benzene-derived graphite fibers provide an excellent host material for a structural analysis of both the intercalation and ion-implantation processes in graphite. Using the *c*-axis lattice imaging technique, with a high-resolution electron microscope, we observe well-staged intercalated regions in this fiber matrix. With regard to ion implantation, we find a distribution in the density of lattice defects with depth from the fiber surface. Ion implantation is also found to increase the graphite interlayer spacing. This information is correlated with electrical properties of these fibers.

### INTRODUCTION

Graphite fibers with the highest structural perfection yet achieved have been successfully fabricated by thermal decomposition of a mixture of benzene and hydrogen gas<sup>1-3</sup> at a temperature of approximately 1100°C. The fiber axis is oriented along a basal plane direction and the *c* axis is radial.<sup>4</sup> When heat treated to temperatures as high as 2900°C, the fibers exhibit graphite crystallites with dimensions larger than 1000 Å and an unusually high degree of structural order. These fibers also have the highest electrical conductivity, bulk modulus, and tensile strength yet found in fibrous graphite materials.<sup>4-8</sup> Furthermore, for fibers with diameters less than 0.8  $\mu\text{m}$ , the *c*-axis lattice image and defect structures can be observed directly using high-resolution electron microscopy without any thinning and sectioning or special sample preparation. Thus benzene-derived fibers (BDF), heat treated to 2900°C and above, provide an excellent matrix for the study of structural order associated with the intercalation and implantation processes.

It has been previously shown using Debye-Scherrer x-ray diffraction and Raman spectroscopy that well-staged GIC (graphite intercalation compounds) with Rb, AlCl<sub>3</sub>, SbCl<sub>5</sub>, FeCl<sub>3</sub>, CoCl<sub>2</sub>, NiCl<sub>2</sub>, and KHg intercalants can be synthesized in the fiber matrix, when previously heat treated to heat-treatment temperatures ( $T_{\text{HT}}$ ) of 2900°C and above.<sup>7-9</sup> Little evidence for well-staged acceptor GIC has been found in polyacrylonitrile (PAN) or mesophase pitch-based carbon fibers.<sup>10</sup>

The first focus on the present work is the direct observation using the lattice fringe imaging technique of *c*-axis

lattice planes corresponding to well-staged regions of donor (K) and acceptor (FeCl<sub>3</sub> and CuCl<sub>2</sub>) GIC in this fiber matrix. The observed *c*-axis spacing in a stage-1 potassium-intercalated graphite fiber is 5.46 Å and that in a stage-1 FeCl<sub>3</sub>-intercalated graphite fiber is 9.34 Å. The electrical resistivity for these pristine and intercalated fibers has been measured over a wide temperature range  $4 < T < 1100 \text{ K}$  in an argon atmosphere. A metallic temperature dependence is found in both the pristine and intercalated BDF. The acceptor intercalants studied in this work yield air-stable fibers which are also thermally stable up to about 320°C for the FeCl<sub>3</sub> system and to about 200°C for the CuCl<sub>2</sub> system.

The second focus of this work is the direct observation by the lattice fringe imaging technique of defect structures created by the implantation of tin ions into these well-ordered graphite fibers. The results show a distribution in the defect density with depth and an enlargement in the *c*-axis graphite spacing from  $d = 3.36 \text{ Å}$  to  $d$  as large as  $3.9 \pm 0.1 \text{ Å}$ . A temperature-dependent resistivity curve for a boron-implanted benzene-derived fiber ( $T_{\text{HT}} = 3500^\circ\text{C}$ ) is compared to that of the original BDF, showing a degradation in conductivity upon implantation because of ion beam-induced structural defects.

### EXPERIMENTAL

The pristine graphite fibers used in this study were derived from a benzene precursor material,<sup>1-3</sup> and subsequently heat treated at temperatures of 2900°C and 3500°C. The intercalation of these fibers was performed using the two-zone growth technique.<sup>11-13</sup> The stage-1

K-intercalated BDF was prepared with the fibers maintained at 280°C and the prepurified potassium metal at 250°C for a period of ~4 days; the resulting fibers were a golden color following intercalation. The stage index and staging fidelity were investigated in similarly prepared fiber samples by Debye-Scherrer x-ray diffraction using a Cu  $K\alpha$  source. The diffractograms showed that the fibers were stage-1 material with high staging fidelity. The intercalation of acceptors was performed with an overpressure of Cl<sub>2</sub> gas at 300 Torr in the reaction ampoule.<sup>14</sup>

The tin-implanted fibers were prepared using a 70-keV acceleration voltage and a fluence of 10<sup>14</sup>/cm<sup>2</sup>. Under these conditions, the estimated normal-incidence ion penetration depth  $R_p$  from Lindhard-Scharff-Schiøtt (LSS) theory<sup>15</sup> and ion stopping-power tables is 296 Å with a Gaussian halfwidth  $\Delta R_p$  of 54 Å. For the boron-implanted fibers, the ions were accelerated to 100 keV and the fibers were exposed to a fluence of 2.8 × 10<sup>15</sup> boron ions/cm<sup>2</sup>. In this case,  $R_p \cong 2820$  Å and  $\Delta R_p \cong 500$  Å. Previous work on ion implantation into bulk HOPG (highly oriented pyrolytic graphite) has shown the applicability of LSS theory to this crystalline host material.<sup>16</sup>

Because of their small diameters (~1 μm), the fibers require no special sectioning or microtoming for electron microscopy observations. For the case of K-intercalated fibers which desorb readily in air, the fibers were mounted on a folding copper grid in an argon atmosphere within a glove bag onto a single-tilt sample holder. The holder was subsequently introduced into the goniometer stage with a maximum exposure time to air of less than 0.5 sec. Some color change occurred during the sample handling prior to loading into the microscope. In contrast, for the case of FeCl<sub>3</sub>- and CuCl<sub>2</sub>-intercalated fibers, they were mounted on a folding grid in air because these samples are relatively air stable.

The lattice images were obtained using a JEOL 200 CX electron microscope with high resolution pole pieces ( $C_s = 2.8$  mm) and a LaB<sub>6</sub> filament. The observed point-to-point resolution with this stage was 2.9 Å. Because the LaB<sub>6</sub> filament is a bright electron source, exposure times used for recording the image could be as short as 4 sec at a magnification of 650 000×. The images were recorded on Kodak SO-163 electron microscope film. A typical acceleration voltage was 200 keV with a condenser aperture of 300 μm. The amount of decomposition, beam-induced damage, or vacuum desorption of the intercalant in the compound under observation was small, based on the quality of the lattice fringe images and the reproducibility of the observations on specimens from different batches.

The suitable areas of the fiber specimen for lattice imaging are the edge regions of the fiber, several hundred Å from the fiber surface. In this region, we selected an area of the sample where the sample thickness was less than ~500 Å. The graphite layer planes in these regions are oriented such that the (00 $l$ ) diffraction pattern is always observed under axial illumination. The lattice images were obtained with the circular objective aperture positioned to encompass, at minimum, the (000) and (002) reflections observed in the back focal plane of the objective lens. The truncation of the Fourier series corresponding to the selected area enhances the contrast to the spatial

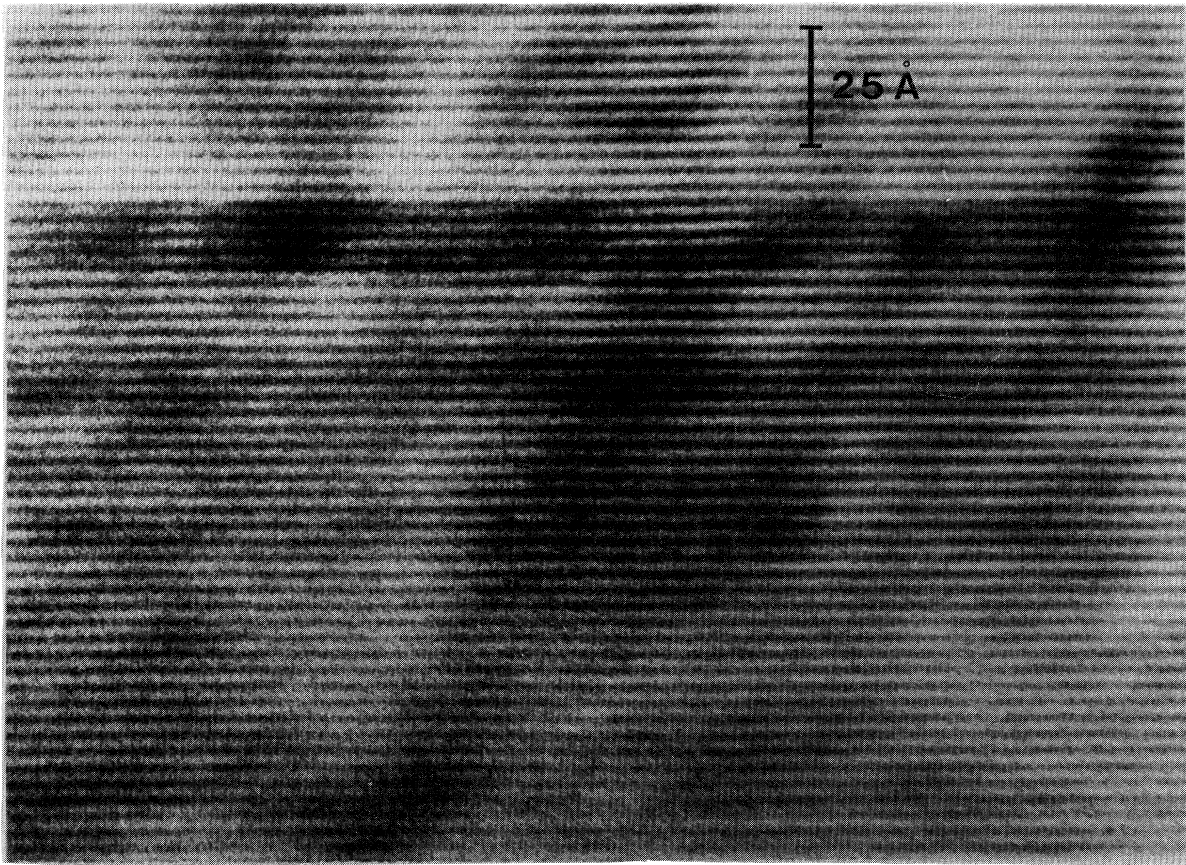
frequencies of interest in the observed real-space image. The interlayer spacing of lattice fringes in intercalated fibers was determined by taking an optical interferogram<sup>17</sup> of the electron micrograph, and using the pristine fiber interlayer spacing of 3.36 Å as a reference.

The electrical resistivity of single fibers was measured by a conventional four-terminal method similar to that used previously.<sup>7-9</sup> For the high-temperature resistivity measurements above room temperature, special gold paste was used to form the electrical contacts between the sample and lead wires, and the measurements were carried out in an argon atmosphere to prevent oxidation from occurring.

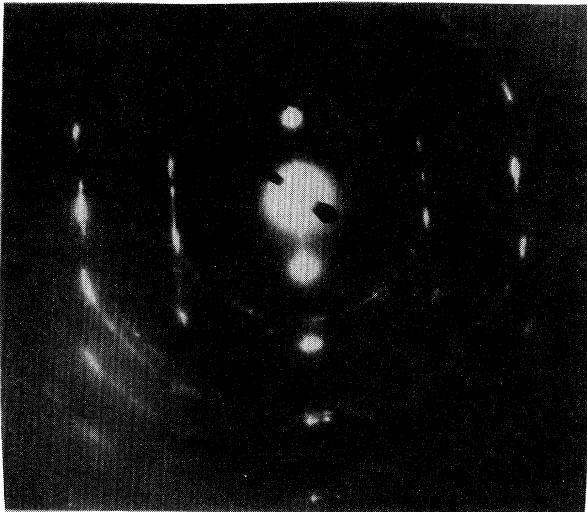
## RESULTS AND DISCUSSION

Figure 1(a) shows a typical (002) lattice fringe image obtained from a pristine benzene-derived fiber heat treated to 2900°C. The selected area diffraction (SAD) pattern shown in Fig. 1(b) exhibits sharp ( $hkl$ ) reflections corresponding to the three-dimensional graphite structure. The observed (00 $l$ ) reflections are characteristic of a monocrystalline sample, suggesting that the graphite layers are oriented in planes parallel to the fiber axis. It has already been shown that upon heat treatment, the basic graphite annular ring structure along the fiber axis is maintained and that the fiber cross section is faceted.<sup>4,8</sup> Large defect-free regions can be inferred from the (002) lattice image shown in Fig. 1(a) where the straight graphite fringes are found to extend over macroscopic dimensions (> 1000 Å) in both  $a$ -axis and  $c$ -axis directions. The lattice fringe images in the fiber host material appear similar to those observed for single-crystal graphite.<sup>18</sup> The analysis of the lattice fringe pattern is made with the optical interferogram shown in Fig. 1(c) which exhibits only the 3.36-Å  $c$ -axis periodicity of the graphite lattice.

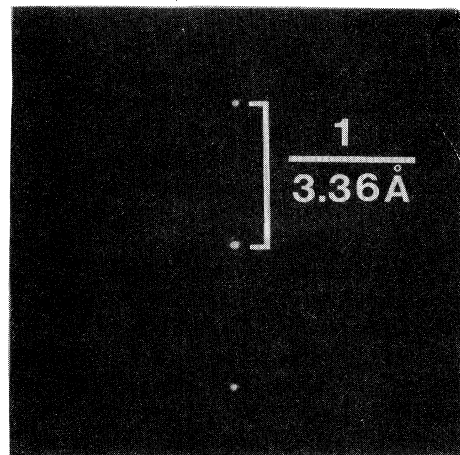
This result obtained on a pristine fiber with  $T_{HT} = 2900^\circ\text{C}$  is very similar to that previously reported for fibers with  $T_{HT} = 2800^\circ\text{C}$ .<sup>19</sup> It has however been shown with measurements of the temperature dependence of the electrical resistivity, the magnetoresistance, and second-order Raman scattering<sup>4,7,8</sup> that the crystalline ordering improves significantly as the heat-treatment temperature is increased from 2800°C to 2900°C and above. Because of the long lengths of the defect-free regions for the fibers heat treated to 2900°C, Debye-Scherrer x-ray diffraction techniques are relatively insensitive for distinguishing between the high degree of structural ordering in the 2900°C fibers and fibers heat treated to higher temperatures. Also, because of the low density of defects found in fibers heat treated to 2900°C, the  $c$ -axis lattice fringe imaging technique is not appropriate for distinguishing between the 2900°C fibers and fibers heat treated to even higher temperatures. For these reasons and others given below, the pristine fibers with  $T_{HT} = 2900^\circ\text{C}$  were chosen as the reference material for the lattice imaging results in this work. High-temperature heat treatment above 2900°C is complicated by the vaporization of the graphite susceptor and of the fibers. In spite of precautions, carbon transport generates sooty deposits which



(a)



(b)



(c)

FIG. 1. (a) Lattice fringe image of a pristine benzene-derived fiber heat treated to 2900 °C. (b) Selected area diffraction pattern corresponding to this lattice image. (c) Optical interferogram taken from the pattern in (a).

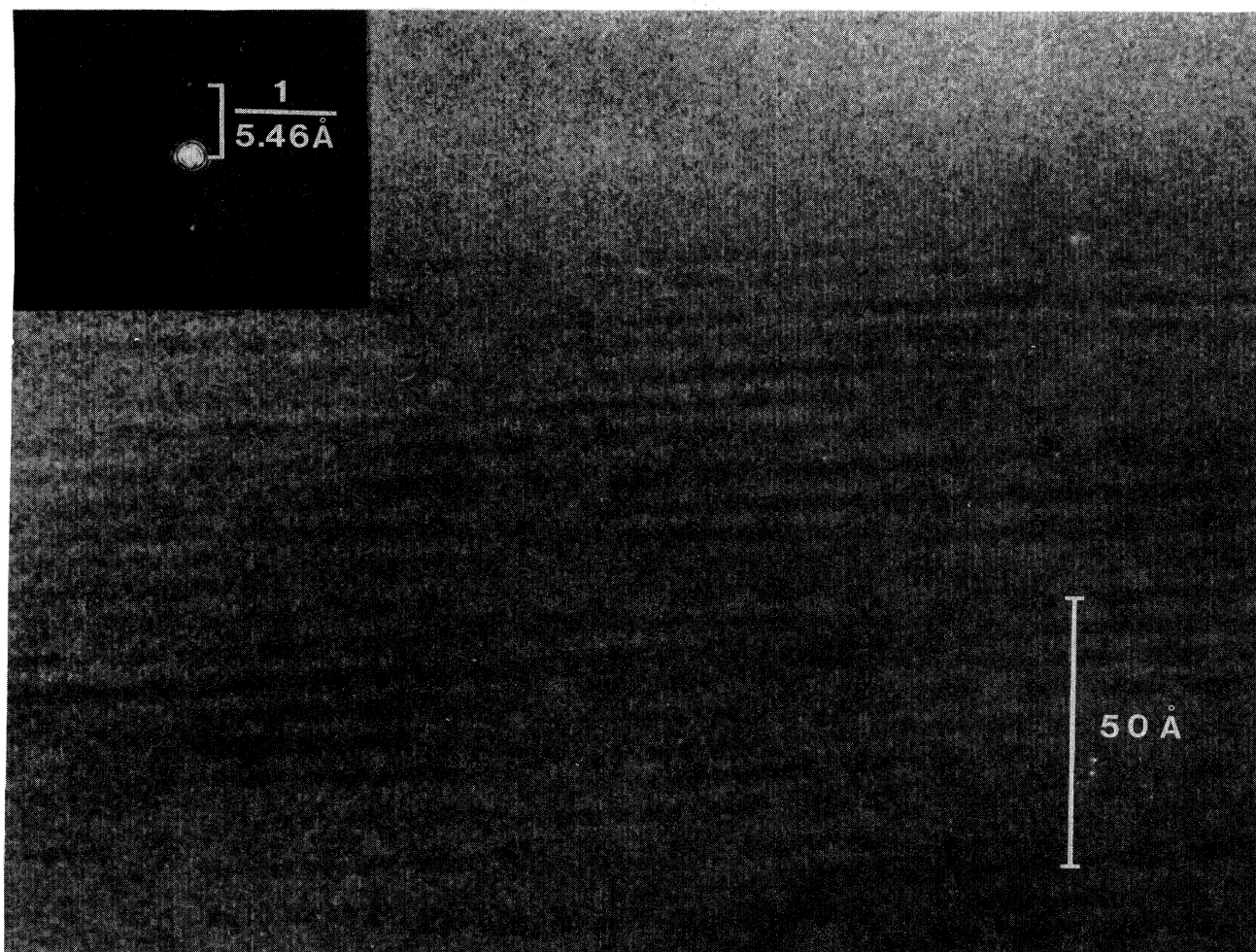


FIG. 2. High-resolution lattice fringe image of a well-ordered stage-1 compound formed by intercalating potassium into benzene-derived fibers ( $T_{HT} = 2900^\circ\text{C}$ ). An optical interferogram taken from the lattice fringe pattern is shown in the inset.

bond a portion of the fiber samples to the sample holder, thereby obscuring temperature measurement by a pyrometer.<sup>8</sup> Uncertainty in the heat-treatment temperatures arising from the sooty deposits and from variations in the uniformity of the temperature in the furnace is estimated to be as much as 2%.

Figure 2 shows the (00 $l$ ) lattice image of a potassium-intercalated benzene-derived fiber ( $T_{HT} = 2900^\circ\text{C}$ ). In this figure, the lattice fringes clearly exhibit stage-1 material with a characteristic interlayer spacing of 5.46 Å as determined by the optical interferogram shown in the inset. This value correlates well with previously reported values for  $I_c$  in the range  $5.35 \leq I_c \leq 5.40$  Å in stage-1 potassium intercalated graphite based on an HOPG host material.<sup>20</sup> It is seen in Fig. 2 that after intercalation, the fibers maintain the same basic fibrous form. Noteworthy is the increased linewidth of the (00 $l$ ) x-ray reflections in the intercalated fibers relative to that found in the pristine material, indicating a reduction in crystallite size in the  $c$ -axis and  $a$ -axis directions subsequent to intercalation; this is corroborated by the observed lattice fringes (see Fig. 2). The staging fidelity as well as the  $c$ -axis crystallite size in

the intercalated fiber are directly determined from the lattice fringe image and are corroborated by Debye-Scherrer x-ray diffraction measurements. The parallel stacking of the fringes corresponding to the intercalated crystallite is about three to four layers ( $\sim 20$  Å) on average, while an estimate of the coherence length taken from the full width at half maximum of the (002) Debye-Scherrer x-ray diffraction peak is  $\sim 70$  Å. This discrepancy in  $c$ -axis crystallite thickness between these two measurements can be understood from the relative insensitivity of the x-ray analysis to small crystallite misorientations, because the x-ray results provide information averaged over many lattice planes while the high-resolution electron microscopy results provide a nonstatistical evaluation of the microstructure of the material.

The observations in Fig. 2 are contrary to previous results,<sup>21–24</sup> especially those obtained by Evans and Thomas in powdered natural graphite<sup>21</sup> where the potassium was observed to be randomly staged in the graphite matrix. Furthermore, the lattice fringe image of Fig. 2 shows that the  $c$  axis of the crystallite is oriented nearly perpendicular to the fiber axis. The average length of the lattice fringes,

corresponding to the in-plane crystallite dimension, is found to be about 50–80 Å. The degradation of the  $a$ -axis crystallite size after K intercalation is consistent with the observation by Evans and Thomas on a single crystal Ticonderoga potassium-intercalated graphite compound.<sup>21</sup> An estimate of the in-plane crystallite dimension taken from the  $(10\bar{1}0)$  lattice image reported by these authors is about 50 Å, in good agreement with the result obtained from the present fibrous host material. Mixed staging, showing adjacent regions of stage-1 and of higher-stage material, is frequently observed in the same set of samples which show the well-staged behavior of Fig. 2. This observation is similar to that reported by Evans and Thomas,<sup>21</sup> as mentioned above.

For the intercalation of acceptors it has already been shown that well-staged intercalation compounds with  $\text{AlCl}_3$ ,  $\text{FeCl}_3$ ,  $\text{SbCl}_5$ ,  $\text{CoCl}_2$ , and  $\text{NiCl}_2$  (Refs. 7–9) can be readily synthesized in this fiber (BDF) matrix when heat treated to 2900°C. In the present work, particular attention has been given to studies on *air-stable* intercalants such as  $\text{FeCl}_3$  and  $\text{CuCl}_2$  because it is these intercalated fibers which are expected to be of greatest interest for practical applications.

Figure 3 shows the (002) lattice fringe image for an  $\text{FeCl}_3$ -intercalated benzene-derived fiber ( $T_{\text{HT}}=2900^\circ\text{C}$ ). In this case, the lattice fringes exhibit single stage-1 fiber regions with a characteristic interlayer spacing  $I_c=2d=9.34$  Å where  $d=4.67$  Å is the fringe spacing as determined by an optical interferogram. Since the lattice fringes were formed from beams up to (002), higher-order Fourier components were produced in the lattice fringes, and hence the smaller  $d$  value. This value of  $I_c$  found from the lattice fringe pattern is in good agreement with the previously reported value of 9.37 Å for  $I_c$  in stage-1  $\text{FeCl}_3$ -intercalated graphite.<sup>20</sup> This is of significance since this work represents the first observation of well-staged, defect-free intercalated regions extending up to dimensions of  $\sim 400 \times 50$  Å<sup>2</sup> in this fibrous host material.

We have also examined the  $c$ -axis lattice structure of a  $\text{CuCl}_2$ -intercalated BDF ( $T_{\text{HT}}=2900^\circ\text{C}$ ). The resulting

lattice fringe image is shown in Fig. 4 with the corresponding (00 $l$ ) SAD pattern. In this case, the lattice fringes show a mixture of stage-1, -2, and higher-stage regions. However, the diffraction pattern shown in the inset clearly exhibits superlattice diffraction spots corresponding to staged compounds. Noteworthy is the observation of regions of well-staged material, extending deep into the bulk for more than 400 Å from the fiber surface and running continuously along the  $a$ -axis direction for more than 800 Å. This observation is corroborated by Debye-Scherrer x-ray diffraction measurements which show that these intercalated fibers are staged into the bulk with no graphite (002) line present in the x-ray diffraction pattern.

Based on the above observations, it is seen that intercalation with the acceptors  $\text{FeCl}_3$  and  $\text{CuCl}_2$  does not greatly degrade the  $c$ -axis and  $a$ -axis crystallite sizes in the present fibrous host material previously heat treated to 2900°C. In particular, this observation is in contrast to the  $c$ -axis lattice fringing results obtained by Thomas *et al.*<sup>22</sup> in powdered natural graphite intercalated with  $\text{FeCl}_3$ , which did not show such a high degree of ordering.

The results of Figs. 3 and 4 are pertinent to the explanation of the high electrical conductivity and the metallic temperature dependence found in these intercalated fibers as shown in Fig. 5 over the temperature range  $4 < T < 600$  K. Both pristine benzene-derived fibers ( $T_{\text{HT}}=2900^\circ\text{C}$ ) and intercalated BDF show a metallic temperature dependence of the resistivity with a stronger temperature dependence and a different functional form for the intercalated fibers than for the pristine fibers. It is seen that intercalation results in a decrease in the room-temperature resistivity by a factor of about 10 for the  $\text{FeCl}_3$  intercalant. The absolute values of resistivity for the intercalated BDF at room temperature are comparable with values obtained with these intercalants on HOPG based samples.<sup>20</sup> It is of great practical interest that air-stable fibers with average room-temperature resistivity value as low as  $7 \mu\Omega \text{ cm}$  can be achieved in  $\text{FeCl}_3$ -intercalated BDF. This resistivity value corresponds to a conductivity per mass-density ratio comparable to that of copper.

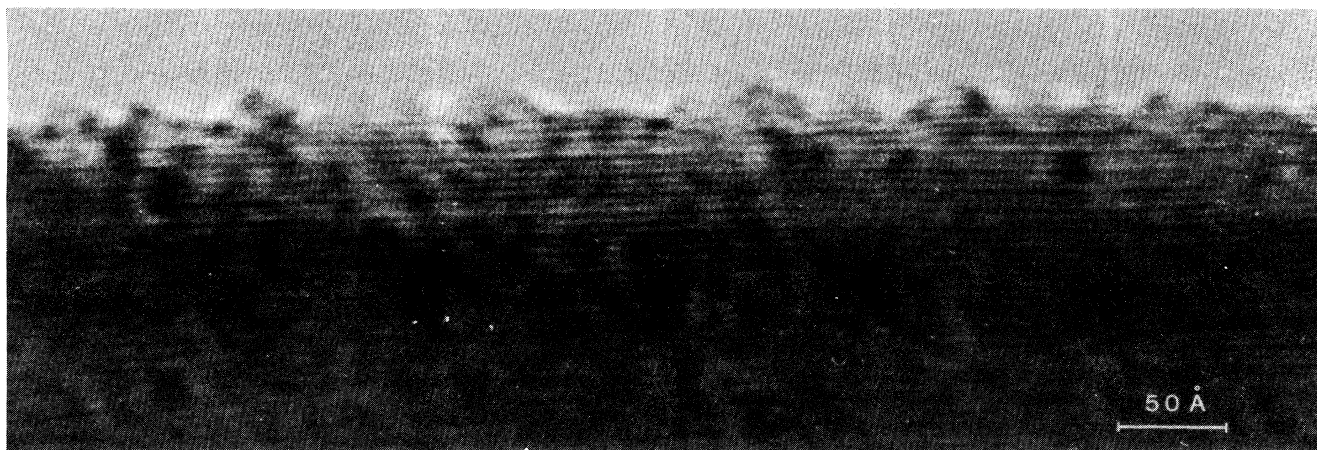


FIG. 3. High-resolution lattice fringe image of a stage-1  $\text{FeCl}_3$ -intercalated benzene-derived fiber ( $T_{\text{HT}}=2900^\circ\text{C}$ ) showing a well-ordered, single-staged region of dimensions  $50 \times 400$  Å<sup>2</sup>.

The data presented in Fig. 5 represent an average of resistivity measurements for a number of samples ( $\sim 8$ ) prepared from the same group of pristine fibers with  $T_{HT}=2900^\circ\text{C}$ . The lowest room-temperature resistivity measured for an individual  $\text{FeCl}_3$ -intercalated BDF was  $5.1 \mu\Omega \text{ cm}$ . The experimental scatter in the group of eight samples used to obtain the data of Fig. 5 was  $\sim 30\%$ . Because of the stage dependence of the resistivity, a variation in resistivity of  $\sim 40\%$  from one fiber sample to another can be expected, if we attribute this scatter to differences in stage index and stage fidelity from one fiber to another for stages  $1 \leq n \leq 3$ .<sup>25</sup> To observe the temperature dependence more clearly, a linear plot of the resistivity versus temperature is also shown in Fig. 6.

The unusual temperature dependence of the resistivity of the pristine BDF ( $T_{HT}=2900^\circ\text{C}$ ) is interesting in its own right. Of some practical importance may be the very weak temperature dependence of  $\rho$  in the range  $100 \leq T \leq 400 \text{ K}$ . The relatively weak temperature dependence of resistivity up to  $1100 \text{ K}$  (with a linear temperature coefficient of  $\sim 0.08 \mu\Omega \text{ cm/K}$  for  $400 < T < 1100 \text{ K}$ ) and the good mechanical properties of the BDF at elevated temperatures suggest practical application of the BDF for high-temperature electrical conductors.

The increase in resistivity with temperature for both  $\text{FeCl}_3$ - and  $\text{CuCl}_2$ -intercalated BDF is found to follow approximately the functional form  $\rho(T)=A+BT+CT^2$  used previously by several authors studying  $\rho(T)$  for

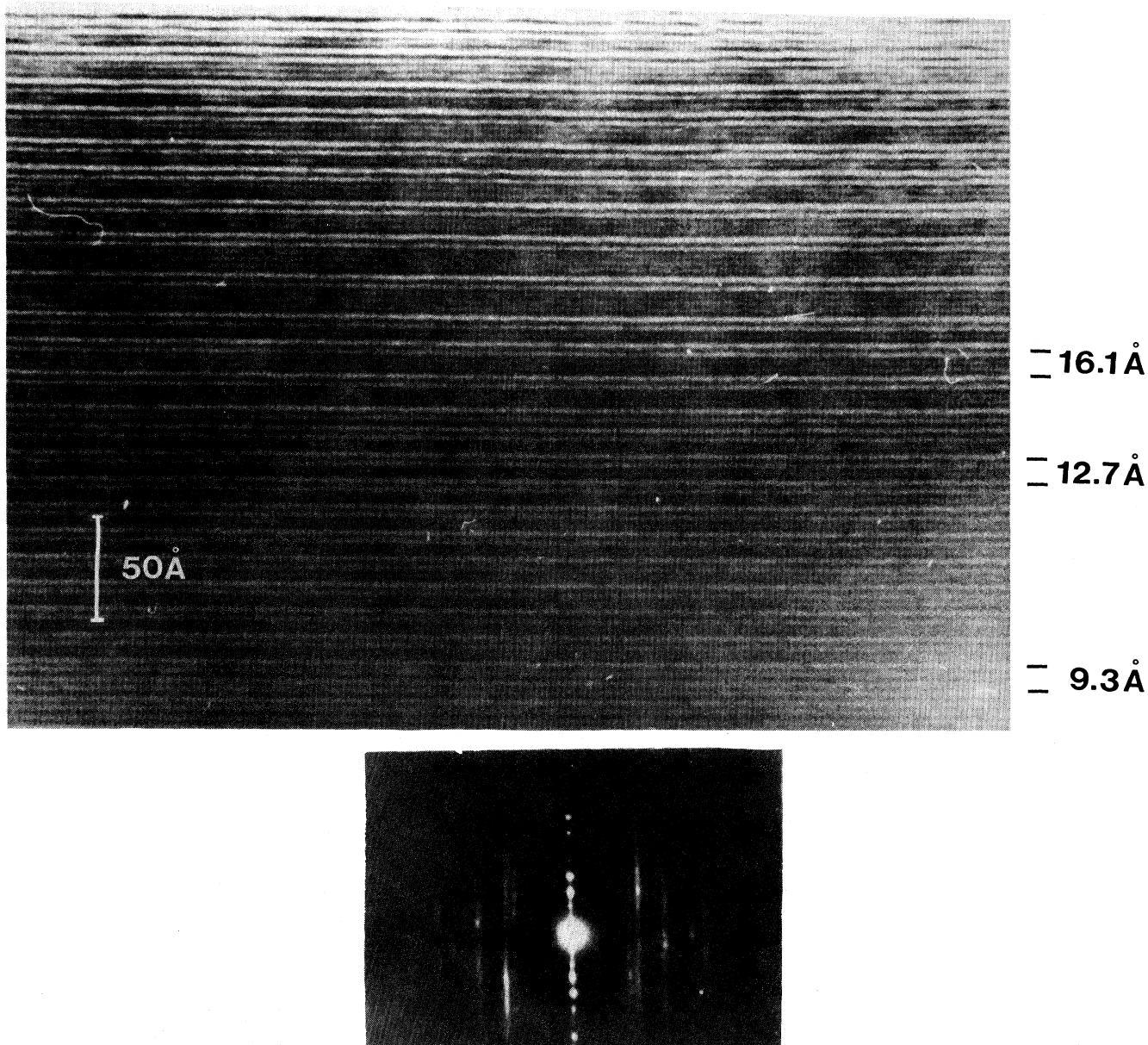


FIG. 4. Lattice fringe image of a  $\text{CuCl}_2$ -intercalated benzene-derived fiber ( $T_{HT}=2900^\circ\text{C}$ ) and the corresponding selected area diffraction pattern.

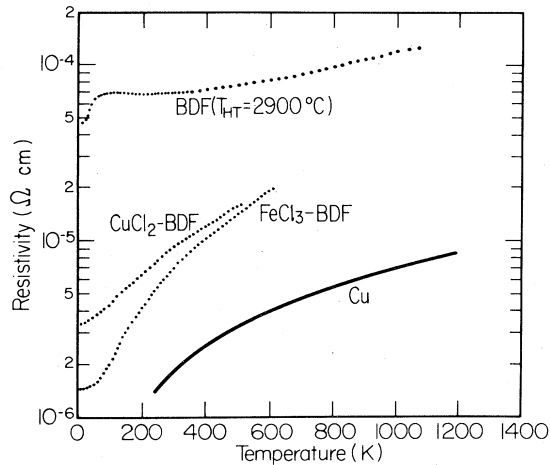


FIG. 5. Semilog plot of the temperature dependence of resistivity in the range  $4 < T < 1100$  K, for pristine fibers ( $T_{HT}=2900^\circ\text{C}$ ) and for the same fibers intercalated with air-stable acceptors ( $\text{FeCl}_3$ ,  $\text{CuCl}_2$ ). A curve for pure copper is included for comparison.

HOPG.<sup>20</sup> For the case of the intercalated fibers, we find  $A = 1.12 \mu\Omega \text{ cm}$ ,  $B = 5.21 \times 10^{-3} \mu\Omega \text{ cm/K}$ , and  $C = 4.83 \times 10^{-5} \mu\Omega \text{ cm/K}^2$  for the  $\text{FeCl}_3$  system and  $A = 3.10 \mu\Omega \text{ cm}$ ,  $B = 7.67 \times 10^{-3} \mu\Omega \text{ cm/K}$ , and  $C = 4.40 \times 10^{-5} \mu\Omega \text{ cm/K}^2$  for the  $\text{CuCl}_2$  system.

The resistivity of these materials is predominantly due to phonon scattering plus scattering due to defects and impurities. Phonon scattering is controlled by the structure and bonding of the material, but defect scattering can be reduced by improving the structural ordering of the original host material. The high electrical conductivity achieved in the present intercalated BDF is thus associated with the structural perfection of the original fibrous host material, as evidenced by the direct observation of the lattice fringe images. This argument is also corroborated by previous magnetoresistance measurements on

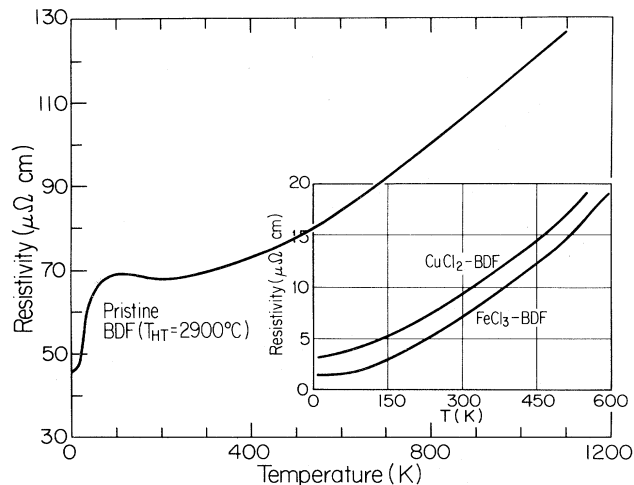


FIG. 6. Linear plot of the temperature dependence of the resistivity for the same fibers as in Fig. 5. Results are shown both for a pristine fiber in the range  $T < 1100$  K, and for the intercalated fibers (lower right-hand inset) in the range  $T < 600$  K.

similarly prepared BDF,<sup>8</sup> which show that the pristine BDF when heat treated to  $2900^\circ\text{C}$  and above have mobilities only a factor of about 7 less than HOPG, and that the benzene-derived fibers intercalated with both donors and acceptor have the same order of magnitude in mobilities as compared to similarly intercalated HOPG. The more rapid increase in resistivity above  $\sim 500$  K in the intercalated fibers may indicate some intercalate desorption, as discussed below.

For practical application of the air-stable intercalated fibers as conductors, their thermal stability is of importance. We have therefore measured the relative change in resistivity  $\Delta\rho/\rho_0 = [\rho(t) - \rho(0)]/\rho(0)$  versus temperature after the sample was held in an argon atmosphere at temperature  $T$  for a time  $t$ . The results are given in Fig. 7 for both the  $\text{FeCl}_3$  and  $\text{CuCl}_2$  systems for  $t = 12$  h. It is of interest to note that essentially no change in  $\Delta\rho/\rho_0$  for the  $\text{FeCl}_3$ -intercalated BDF occurred after long exposures at elevated temperatures for  $T \leq 320^\circ\text{C}$ . From this result it is inferred that intercalant desorption does not significantly degrade the  $\text{FeCl}_3$ -intercalated BDF sample until a temperature of  $\sim 240^\circ\text{C}$  is reached for the  $\text{CuCl}_2$  system and  $\sim 340^\circ\text{C}$  for the  $\text{FeCl}_3$  system. Thus both the magnitude of the room-temperature conductivity and the thermal stability of the  $\text{FeCl}_3$ -intercalated BDF offer promise for the utilization of these fibers as practical lightweight conductors.

With regard to ion-implantation studies, Fig. 8 shows the (002) lattice fringe image pattern of benzene-derived fibers ( $T_{HT}=2900^\circ\text{C}$ ) ion-implanted with tin. It is readily seen that ion implantation degrades the layer ordering of the pristine fibers. Specifically, at a fluence of  $10^{14}$  tin ions/ $\text{cm}^2$ , the parallel stacking of the fringes in Fig. 8 extends for only approximately three layers on average, and the average length of the fringes is about  $50 \text{ \AA}$ . Upon implantation, the interlayer spacing  $d$  between graphite

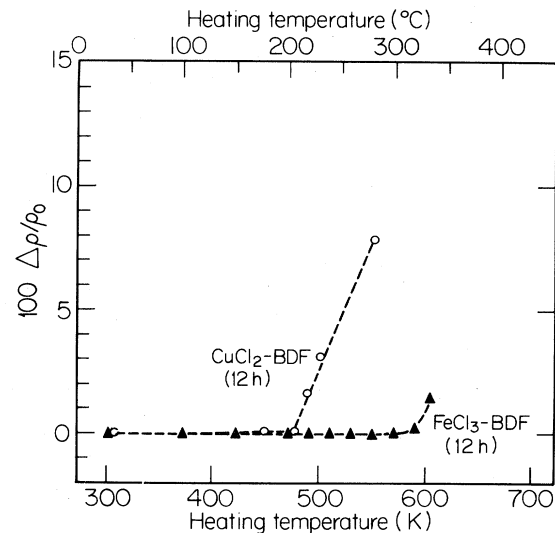


FIG. 7. Relative change in resistivity  $\Delta\rho/\rho_0$  (%) after heating fibers intercalated with  $\text{CuCl}_2$  and  $\text{FeCl}_3$  for 12 h at a temperature  $T$  in the range  $20 < T < 350^\circ\text{C}$ . Electrical contacts are made with gold paste and the measurements are carried out in an argon atmosphere.

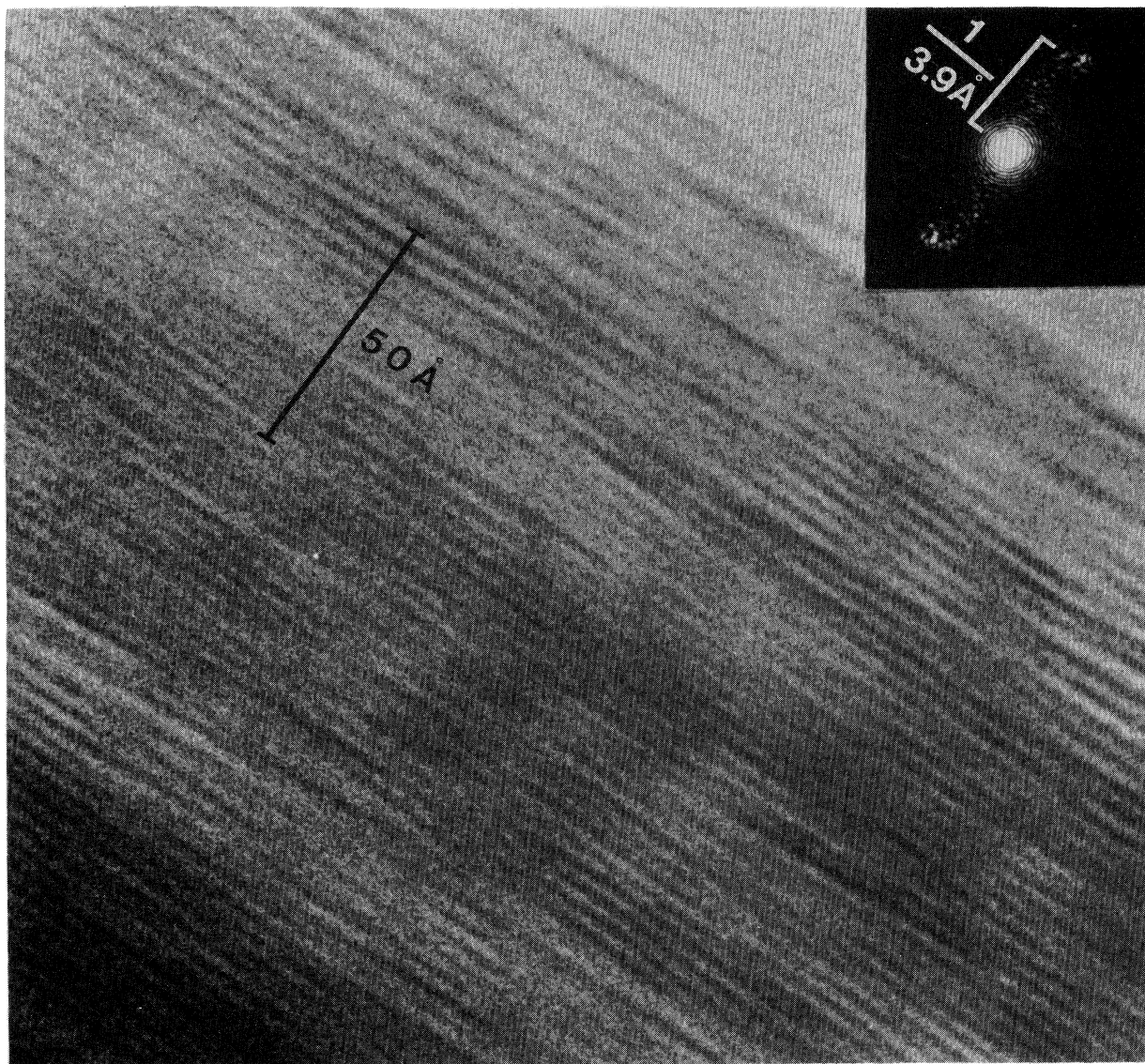


FIG. 8. Lattice image of a tin-implanted benzene-derived fiber ( $T_{HT}=2900^{\circ}\text{C}$ ) (see text). The corresponding optical interferogram showing a large broadening effect of the diffracted spots is presented in the inset.

layers expands between 7% and 14%, and in some regions the expansion yields  $d$  values up to  $\sim 3.9$  Å; the magnitude and range of interlayer spacings was determined from analysis of the optical interferogram shown in the inset of Fig. 8. From the width of the diffraction spot of the optical interferogram, we estimate that the incident ions produce an average misorientation of  $\sim 10^{\circ}$  of the basal plane of the crystallite with respect to the fiber axis. The layer stacking in the interior part of the fiber was observed to remain unaffected by ion implantation; the lattice fringe pattern for the interior of the fiber shows the same stacking texture as the unimplanted fibers. From the micrograph, we estimate the depth of ion penetration to be about 150 Å from the surface of the fiber. The disagreement between this value and  $R_p$  estimated from LSS theory<sup>15</sup> may reflect a departure of the ion beam from normal incidence to the fiber axis.

The effect of ion implantation on the electrical conductivity has also been examined. Explicit results are given for a benzene-derived fiber ( $T_{HT}=3500^{\circ}\text{C}$ ) heavily implanted with  $2.8 \times 10^{15}$  boron ions/cm<sup>2</sup> at 100 keV. The temperature dependences of the resistivity for the same pristine fiber and the boron-implanted fiber are compared in Fig. 9. It is seen that upon implantation of the fiber, the room-temperature resistivity increases by about 5% and the residual resistivity ratio ( $R = \rho_{300\text{ K}}/\rho_{4\text{ K}}$ ) decreases from  $R = 2.33$  (before implantation) to  $R = 1.78$  (after implantation). Also, the temperature dependence of the resistivity changes its functional form and gradually approaches that of fibers with a lower heat-treatment temperature (e.g.,  $T_{HT}=2900^{\circ}\text{C}$ ) showing a flat maximum in resistivity at about 120 K and a shallow minimum at about 220 K. The results are consistent with the introduction of structural defects by ion implantation into the

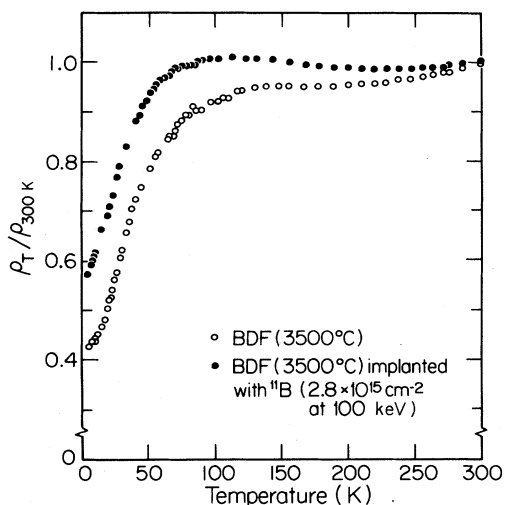


FIG. 9. Temperature dependence of resistivity for a pristine benzene-derived fiber ( $T_{HT}=3500^{\circ}\text{C}$ ) and for the same fiber implanted heavily with boron.

fiber, as evidenced by the direct observation of defect structures in Fig. 8. A summary of the residual resistance ratios for BDF, intercalated BDF, and ion-implanted BDF is given in Table I.

In conclusion, the high structural order and small fiber diameters that can be achieved with the benzene-derived fibers facilitate structural studies of the intercalation and implantation processes using high-resolution lattice fringe imaging. For both processes, lattice fringe imaging provides direct information on the induced structural defects; such information is directly related to the electrical trans-

TABLE I. Summary of the residual resistance ratio ( $\rho_{300\text{ K}}/\rho_{4\text{ K}}$ ) for pristine benzene-derived fibers (BDF), intercalated BDF, and ion-implanted BDF.

Fiber type ( $T_{HT}$ )	( $\rho_{300\text{ K}}/\rho_{4\text{ K}}$ )
BDF ( $2900^{\circ}\text{C}$ )	1.51
Desorbed Rb-intercalated BDF ( $2900^{\circ}\text{C}$ )	5.7
$\text{FeCl}_3$ -intercalated BDF ( $2900^{\circ}\text{C}$ )	4.6
$\text{CoCl}_2$ -intercalated BDF ( $2900^{\circ}\text{C}$ )	3.2
$\text{CuCl}_2$ -intercalated BDF ( $2900^{\circ}\text{C}$ )	2.9
BDF ( $3500^{\circ}\text{C}$ )	2.33
Boron-implanted <sup>a</sup> BDF ( $3500^{\circ}\text{C}$ )	1.78

<sup>a</sup>See text.

port properties of these materials and explains the high electrical conductivities that can be obtained in the intercalated fibers. This work represents the first direct observation of lattice fringe imaging of an intercalation compound, prepared in a fiber host material. The results show well-staged regions extending up to macroscopic dimensions in the case of acceptor compounds.

#### ACKNOWLEDGMENTS

The authors wish to thank Dr. G. Dresselhaus and Dr. P. L. Pober for valuable discussions, National Science Foundation Materials Research Laboratories Grant No. DMR-81-19295 for support of the MIT work. We thank M. Rothman and Dr. J. P. Donnelly (MIT Lincoln Laboratory) for assistance with the ion implantation. We would also like to express our appreciation to Dr. A. W. Moore of Union Carbide for his assistance in the high-temperature heat treatment of the fibers. One of the authors (M.E.) also acknowledges support from the Mitsubishi Foundation.

\*Permanent address.

†Present address: IBM Research Center, P.O. Box 218, Yorktown Heights, NY 10598.

<sup>1</sup>T. Koyama, *Carbon* **10**, 757 (1972).

<sup>2</sup>T. Koyama, M. Endo, and Y. Onuma, *Jpn. J. Appl. Phys.* **11**, 445 (1972).

<sup>3</sup>M. Endo, K. Komaki, and T. Koyama, *International Symposium on Carbon, Tokyo, 1982* (Toyohashi, Tokyo, 1982), p. 515.

<sup>4</sup>M. Endo, Y. Hishiyama, and T. Koyama, *J. Phys. D* **15**, 353 (1982).

<sup>5</sup>T. Koyama and M. Endo, *Jpn. J. Appl. Phys.* **13**, 1175 (1974).

<sup>6</sup>T. Koyama, M. Endo, and Y. Onuma, *Jpn. J. Appl. Phys.* **13**, 1933 (1974).

<sup>7</sup>T. C. Chieu, M. S. Dresselhaus, and M. Endo, *Phys. Rev. B* **26**, 5867 (1982).

<sup>8</sup>T. C. Chieu, G. Timp, M. S. Dresselhaus, M. Endo, and A. W. Moore, *Phys. Rev. B* **27**, 3686 (1983).

<sup>9</sup>T. C. Chieu, G. Timp, M. S. Dresselhaus, and M. Endo, in *Intercalated Graphite*, edited by M. S. Dresselhaus, G. Dresselhaus, J. E. Fischer, and M. J. Moran (Elsevier, New York, 1983), Vol. 20, p. 51.

<sup>10</sup>P. Kwizera, M. S. Dresselhaus, and G. Dresselhaus, *Carbon* **19**, 144 (1981); P. Kwizera, M. S. Dresselhaus, D. R. Uhlmann, J. S. Perkins, and C. R. Desper, *ibid.* **20**, 387

(1982); P. Kwizera, M. S. Dresselhaus, and G. Dresselhaus, *ibid.* **21**, 121 (1983).

<sup>11</sup>J. G. Hooley and M. Bartlett, *Carbon* **5**, 417 (1967).

<sup>12</sup>J. G. Hooley and R. N. Soniassy, *Carbon* **8**, 181 (1970).

<sup>13</sup>P. Kwizera, A. Erbil, and M. S. Dresselhaus, *Carbon* **19**, 144 (1981).

<sup>14</sup>T. C. Chieu, Ph.D. thesis, Massachusetts Institute of Technology, Cambridge, Massachusetts 1983 (unpublished).

<sup>15</sup>J. Lindhard, M. Scharff, and H. E. Schiøtt, *K. Dan. Vidensk. Selsk. Mat. Fys. Medd.* **33**, 14 (1963).

<sup>16</sup>B. S. Elman, M. Shayegan, M. S. Dresselhaus, H. Mazurek, and G. Dresselhaus, *Phys. Rev. B* **25**, 4142 (1982).

<sup>17</sup>G. Timp, M. S. Dresselhaus, L. Salamanca-Riba, A. Erbil, L. W. Hobbs, G. Dresselhaus, P. C. Eklund, and Y. Iye, *Phys. Rev. B* **26**, 2323 (1982).

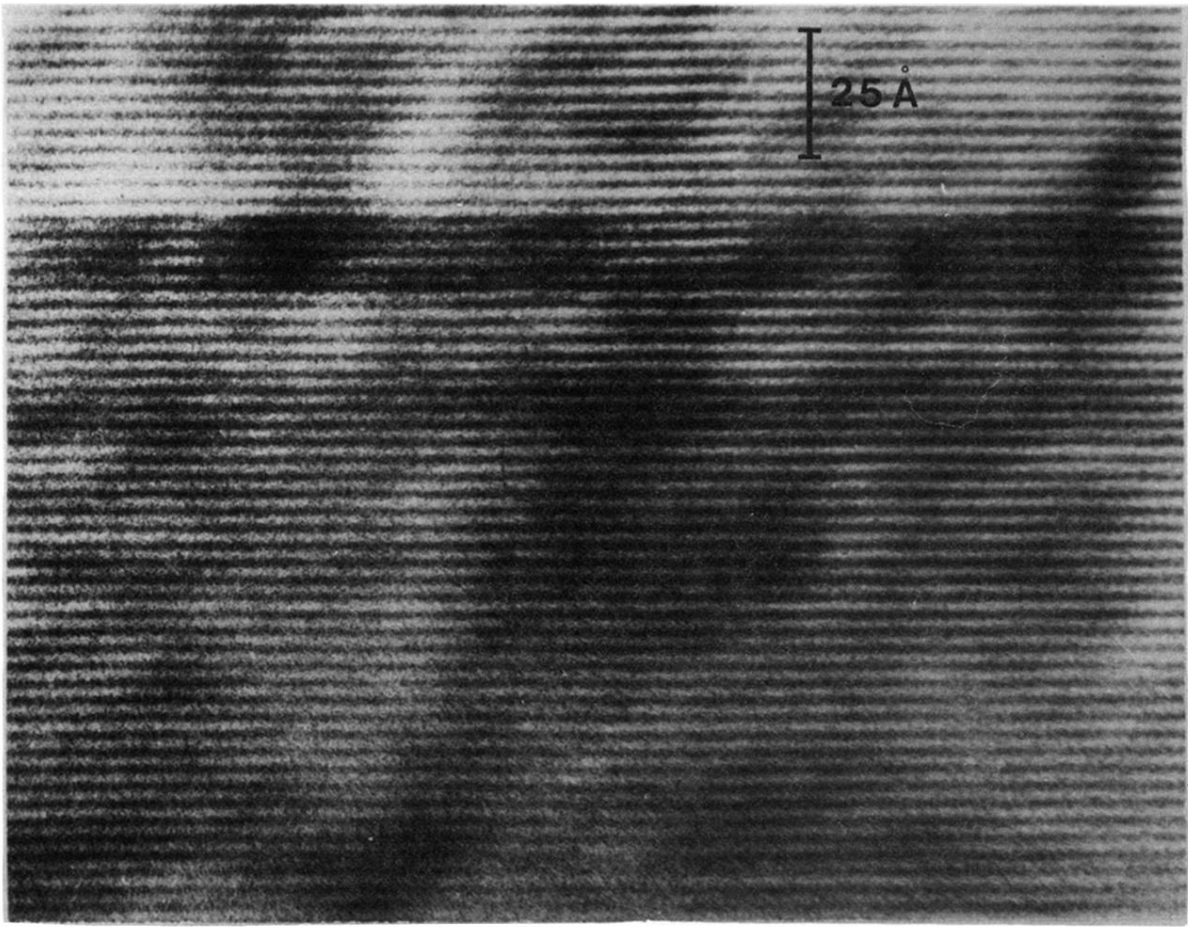
<sup>18</sup>G. R. Millward and D. A. Jefferson, in *Chemistry and Physics of Carbon*, edited by P. L. Walker, Jr. and P. A. Thrower (Dekker, New York, 1980), Vol. 14, p. 1.

<sup>19</sup>M. Endo, A. Oberlin, and T. Koyama, *Jpn. J. Appl. Phys.* **16**, 1519 (1977).

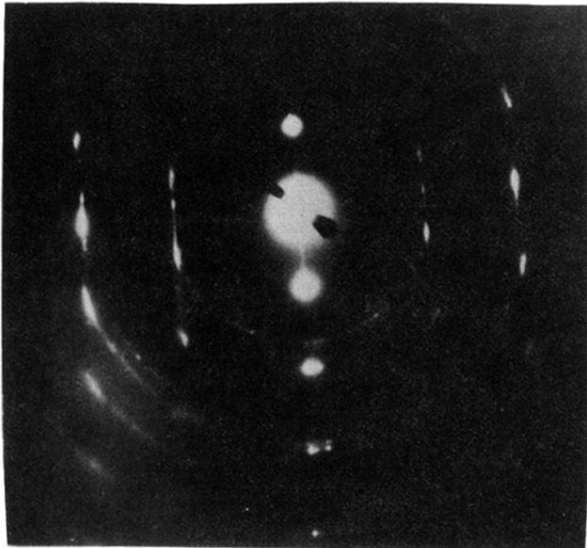
<sup>20</sup>M. S. Dresselhaus and G. Dresselhaus, *Adv. Phys.* **30**, 139 (1981).

<sup>21</sup>E. L. Evans and J. M. Thomas, *J. Solid State Chem.* **14**, 99 (1975).

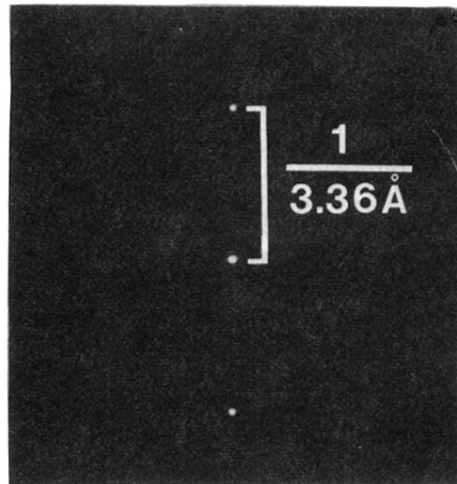
- <sup>22</sup>J. M. Thomas, G. R. Millward, R. F. Schlögl, and H. P. Boehm, *Mater. Res. Bull.* 15, 671 (1980).
- <sup>23</sup>M. M. Heerschap and P. Delavignette, *Carbon* 5, 383 (1967).
- <sup>24</sup>M. M. Heerschap, P. Delavignette, and S. Amelinckx, *Carbon* 1, 235 (1964).
- <sup>25</sup>J.-P. Issi, J. Heremans, and M. S. Dresselhaus, *Phys. Rev. B* 27, 1333 (1983).



(a)



(b)



(c)

FIG. 1. (a) Lattice fringe image of a pristine benzene-derived fiber heat treated to 2900°C. (b) Selected area diffraction pattern corresponding to this lattice image. (c) Optical interferogram taken from the pattern in (a).

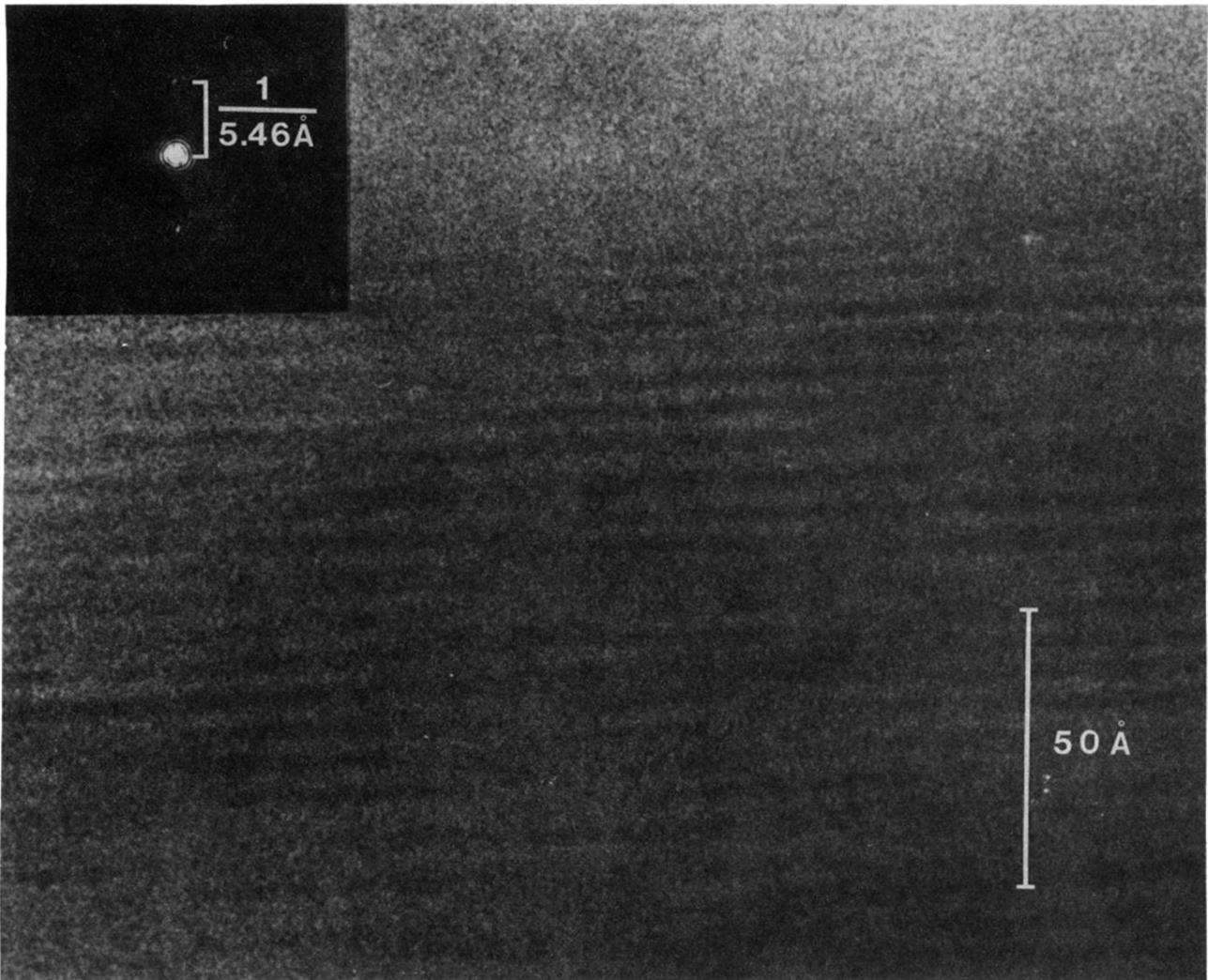


FIG. 2. High-resolution lattice fringe image of a well-ordered stage-1 compound formed by intercalating potassium into benzene-derived fibers ( $T_{HT}=2900^{\circ}\text{C}$ ). An optical interferogram taken from the lattice fringe pattern is shown in the inset.

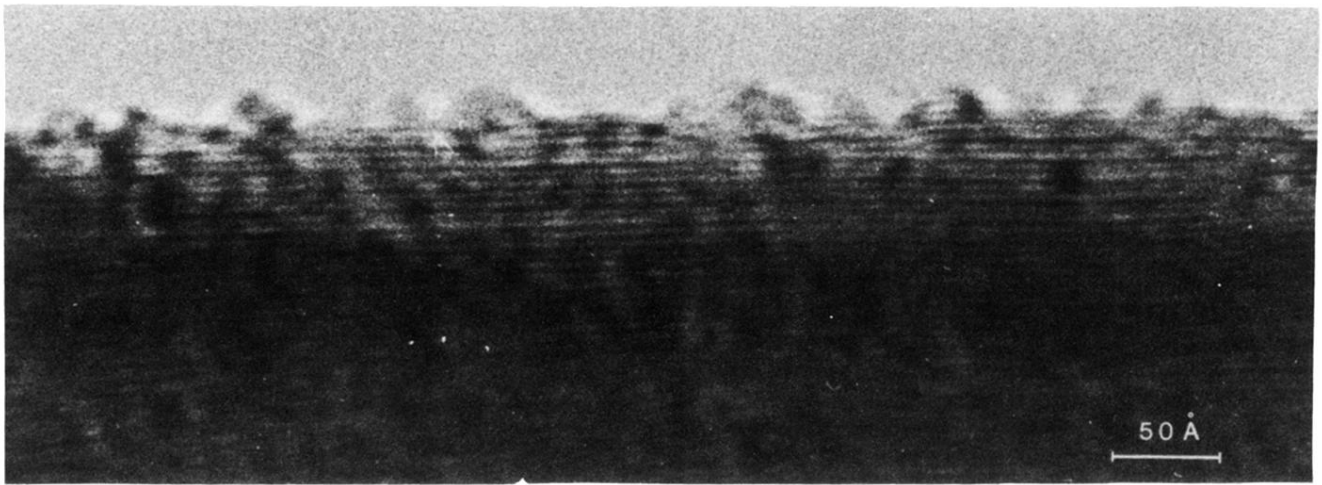


FIG. 3. High-resolution lattice fringe image of a stage-1  $\text{FeCl}_3$ -intercalated benzene-derived fiber ( $T_{\text{HT}} = 2900^\circ\text{C}$ ) showing a well-ordered, single-staged region of dimensions  $50 \times 400 \text{ \AA}^2$ .

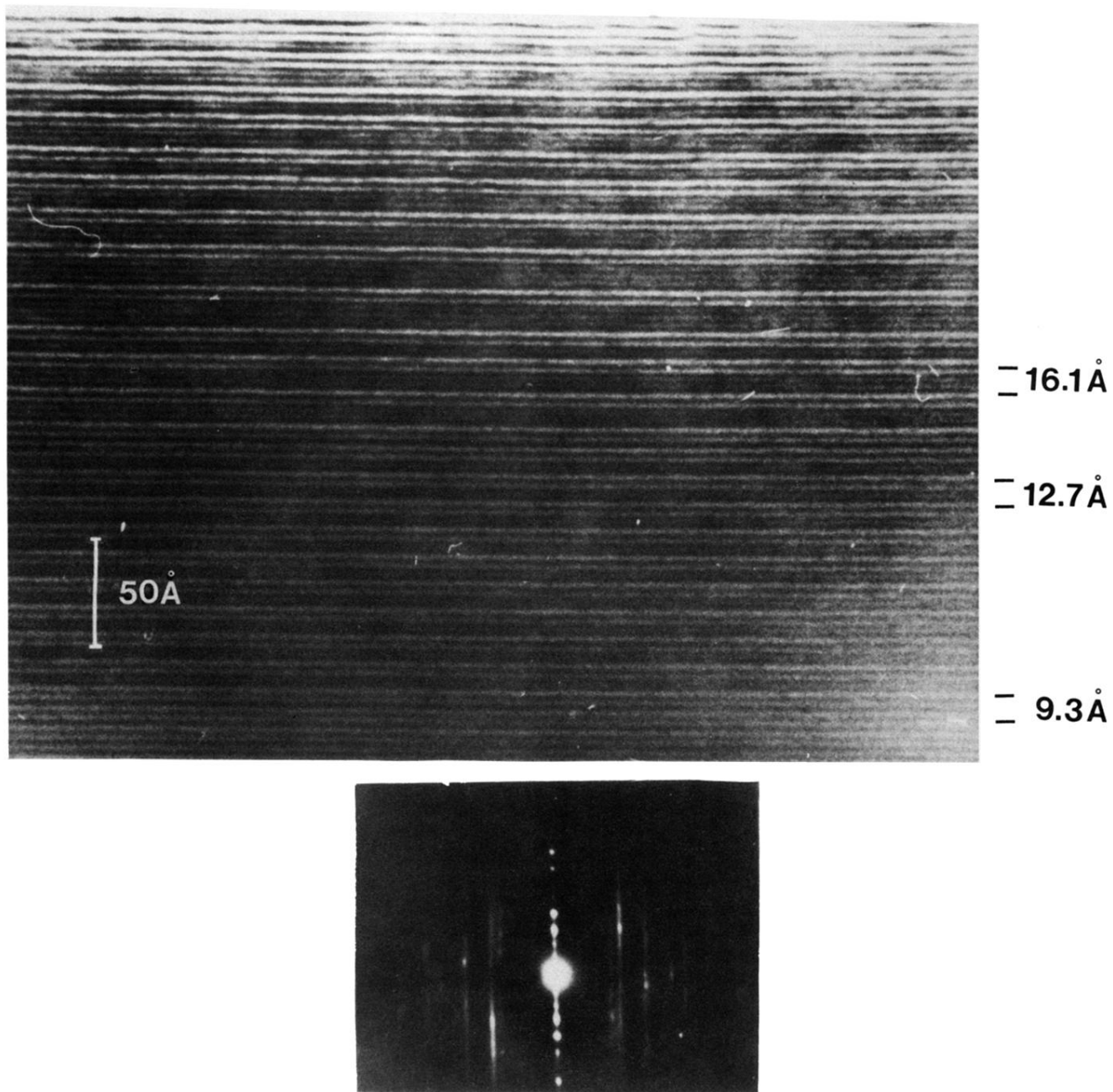


FIG. 4. Lattice fringe image of a  $\text{CuCl}_2$ -intercalated benzene-derived fiber ( $T_{\text{HT}} = 2900^\circ\text{C}$ ) and the corresponding selected area diffraction pattern.

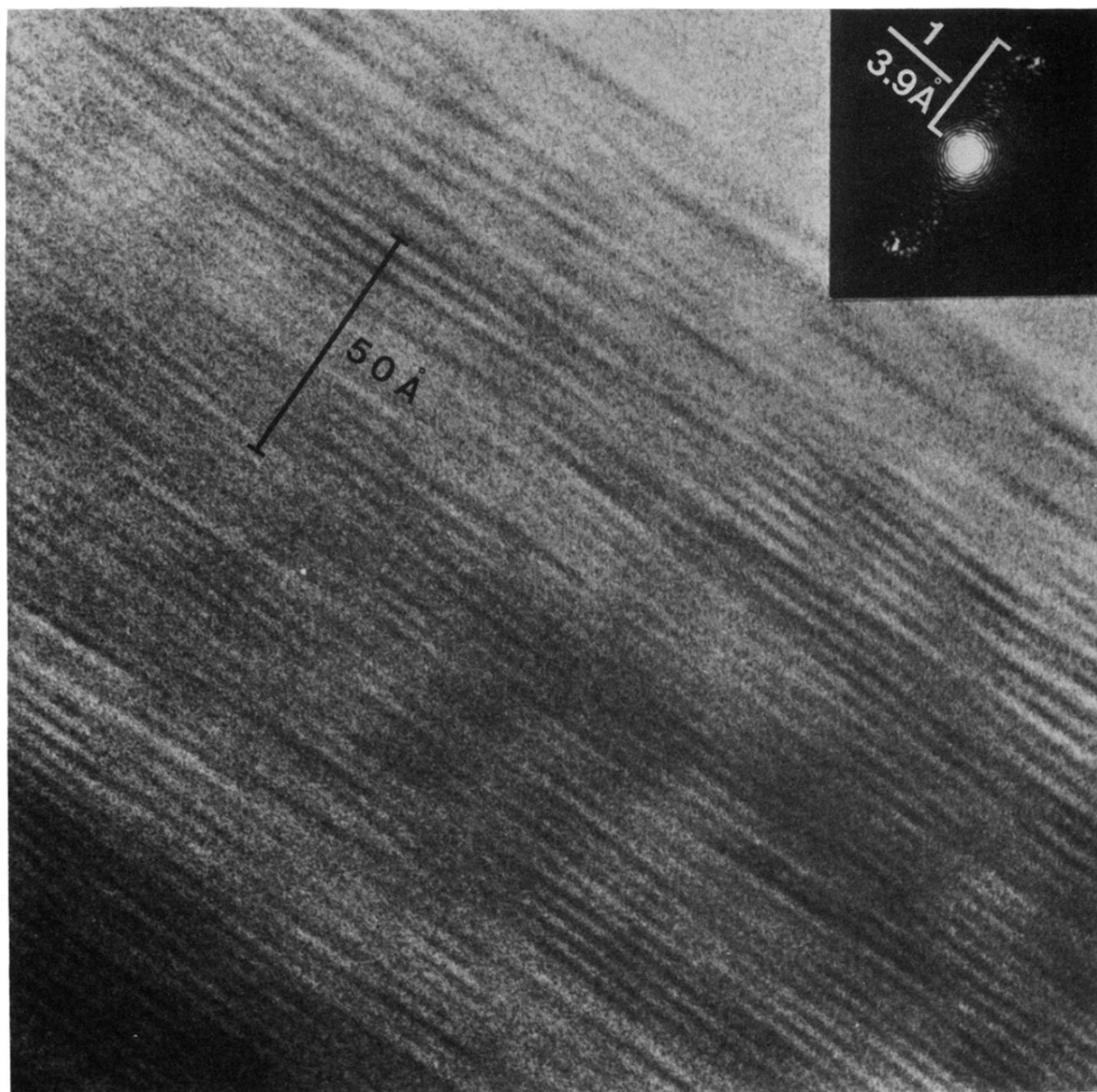


FIG. 8. Lattice image of a tin-implanted benzene-derived fiber ( $T_{HT}=2900^{\circ}\text{C}$ ) (see text). The corresponding optical interferogram showing a large broadening effect of the diffracted spots is presented in the inset.